A NOVEL TOOL FOR UNSUPERVISED FLOOD MAPPING USING SENTINEL-1 IMAGES

D. Amitrano, G. Di Martino, A. Iodice, D. Riccio, G. Ruello

University of Napoli Federico II, Department of Electrical Engineering
and Information Technology, Via Claudio 21, 80125 Napoli, Italy

ABSTRACT

In this paper, we present a novel method for mapping flooded areas exploiting Sentinel-1 ground range detected products. The work introduces two novelties. As first, the input products. In fact, as far we know, no applications using these products has been so far presented in literature. Secondly, a new unsupervised methodology, based on the usage of opportune layers combined in a fuzzy decision system, is presented. Experimental results, obtained both on the single SAR image and on a couple of acquisitions in a change detection framework showed that our method is able to outperform the most popular classification techniques in terms of standard assessment parameters.

Index Terms— Synthetic aperture radar, sentinel-1, flooding, classification, fuzzy systems

1. INTRODUCTION

Floods are among the most serious and frequent natural hazards in the world, causing high damages to people, infrastructure and economies. The UN estimated that about the 56% of the total population affected by weather-related disasters is involved in flood issues (see Figure 1). These events are critical especially in developing countries, but not limited to them. In fact, as an example, in US more than 225 people were killed and more than 3.5 billion dollars in property were damaged by heavy rainfall and flooding each year between 1993 and 1999 [1]. Effective response to floods requires the availability of a map of the affected area in a short time [2].

Synthetic aperture radar (SAR) sensors represent a crucial tool for rapid flooding mapping due to their all-weather and all-time imaging characteristics, ensuring the imaging of the Earth surface independently from illumination and weather conditions. However, information extraction from SAR data is typically considered more difficult by end-users, also due to the lack of dedicated algorithms implemented in some available software suites. As a result, they often prefer to operate with optical/multispectral sensors. In fact, in this case, beyond the possibility to handle images that can be immediately interpreted for visual inspection, very consolidated techniques for the extraction of the flooded area exist, just think

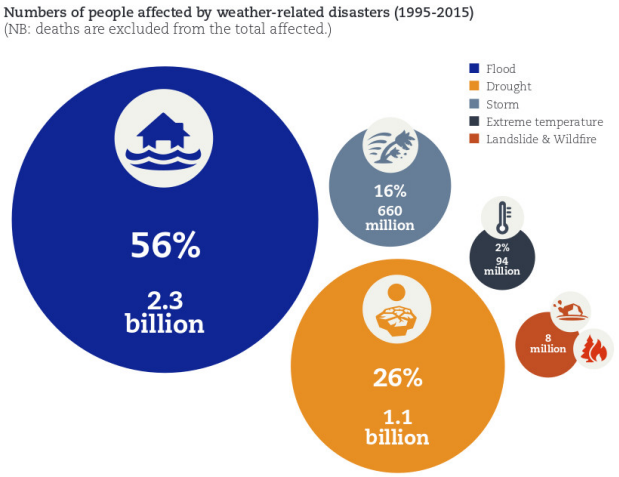

Fig. 1. Number of people affected by weather-related disasters between 1995 and 2015 (source UN).

to the exploitation of the normalized difference water index (NDWI) by McFeeters [3].

However, despite their ease of use and popularity among end-users, multispectral data are often not suitable for emergency due to their sensitivity to weather and illumination conditions. These problems can be overcome using SAR data [4]. In this case, the literature is mainly focused on thresholding-based methods [5, 6]. Here, we introduce a double innovation. The first is at product level. In fact, we exploit Sentinel-1 ground range detected (GRD) products, i.e. detected images pre-processed by ESA and made available to users for download through the Sentinels Data Hub. These products are today still scarcely employed in the SAR literature, despite they are raising a great interest among end-users because they are available for cloud processing within the Google Earth Engine platform [7].

The second innovation is methodological. We propose two processing chains providing maps with increasing resolution. Chain one is based on the analysis of a single GRD product. It exploits classic Haralick textural features [8], and the output is a low resolution map obtainable in few minutes. Chain two is based on change detection. It exploits

the comparison between a couple of GRD products (pre and post-event image) acquired on the same area. The output is map with the same resolution of the input GRD products, i.e. 10 meters.

The work is organized as follows. In Section 2, the proposed methodology is introduced. Experimental results are discussed in Section 3. Conclusions are drawn at the end of the work.

2. METHODOLOGY

Chain one workflow is depicted in Figure 2. The input ia a Sentinel-1 GRD product with 10 meters spatial resolution. It is treated with a 3×3 multilook for speckle reduction, bringing the image resolution to 30 meters. After multilooking, histogram clip is performed to compensate the presence of highly reflecting targets [9]. This allows for for relaxing the pdf of the SAR image, thus enhancing the information content of low reflectivity areas.

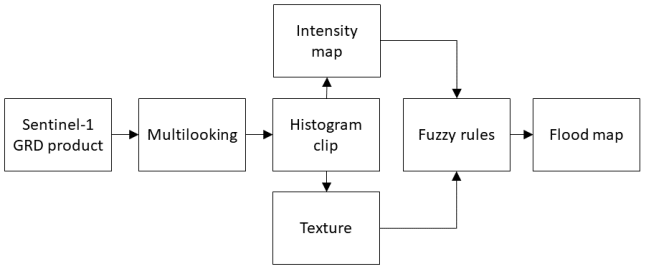

Fig. 2. Flood mapping, chain 1 (single image) workflow. Texture measures in combination with reflectivity information feed a fuzzy classification system for flood area extraction.

Texture processing consists in the calculation of classic Haralick features [8]. Both texture layers and detected image feed the fuzzy decision system. This avoids the search for a thresholding. In fact, the classes "Flood" and "No flood" are automatically assigned through de-fuzzification of the probability maps generated by the fuzzy system. This step is implemented with the maximum membership method [10]. Using a single SAR image, it is necessary to apply masks for the permanent hydrography, otherwise indistinguishable from flooded areas.

The method is fully unsupervised and does not require the application of thresholds. Its processing time is in the order of 30 minutes using a 4-core 32 GB RAM machine.

The change-detection chain is depicted in Figure 3. In this case, the input is a couple of calibrated and coregistered Sentinel-1 GRD products representing the pre- and the post-event scene situation. They are treated with standard despeckling to enhance the contrast between water and land features (here, the refined Lee filter is applied). Filtered images are subject to cross-calibration using the variable amplitude level equalization introduced in [9] in order to ensure that the same object in different images exhibit the same reflectivity. Cross-calibrated images are then used to compute a change index map which, together with the post event image, is used as input layer for the fuzzy decision system.

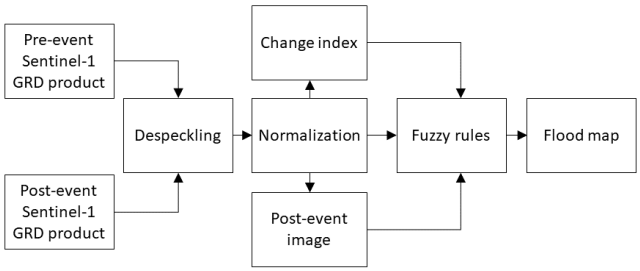

Fig. 3. Flood mapping, chain 2 (change detection) workflow. A couple of calibrated, coregistered product (pre- and post-event image) is exploited to build a change index which, together with post-event amplitude information, feed the fuzzy flood classification system.

The output map has 10 meter spatial resolution, i.e. the full resolution of the GRD product, neglecting possible losses due to the applied despeckling. The method is fully unsupervised , and its processing time mainly depends on the complexity of despeckling. Using the refined Lee filter, the computational time is in the order of one hour and half on a 4-core, 32 GB RAM machine.

3. EXPERIMENTAL RESULTS

The proposed methodology has been tested with several cases taken from the activation list of the Copernicus Emergency Management Service (EMS). This is a wide database, also providing ground truths and masks for the permanent hydrography of the area of interest.

An example of chain 1 result concerning the Jemalong test site (Australia, activation code EMSR184) is reported in Figure 4. In particular, in Figure 3(a), the input product, with the relevant flood map overlaid in cyan color, is shown. The ground truth provided by ESA is displayed in in Figure 3(b).

Qualitatively, a good agreement between the obtained flood map and the available ground truth are registered. We also assessed quantitatively the quality of the generated map using four test sites taken from the Copernicus EMS database. They are: Jemalong, Ballinasloe (Ireland, activation code EMSR149), Selby (UK, activation code EMSR150), Poplar Bluff (US, activation code EMSR176). Results are reported in Table 1. They have been also compared with those given by several literature methods such as k-means, support vector machine (SVM), standard neural network (NN), maximum likelihood (ML) and image thresholding. It arises that our method outperforms the most popular classification tech-

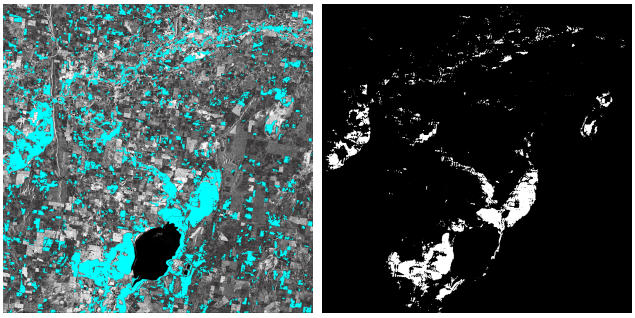

(a) (b)

Fig. 4. Jemalong test site, chain 1 results. (a) Retrieved flood map overlaid to the input GRD product. (b) Ground truth provided by ESA.

niques, allowing for obtaining a high accuracy with negligible incidence of false alarms. In particular, the following average values were obtained for overall accuracy (OA) and false alarms (FA): Proposed method - OA: 93.5%, FA: 6.58%; k-mean - OA: 80.3%, FA: 16.6%; SVM - OA: 78.7%, FA: 3.87%; NN - OA: 49.5%, FA: 3.00%; Threshold - OA: 58.5%, FA: 2.49%; ML - OA: 42.8%, 2.37%.

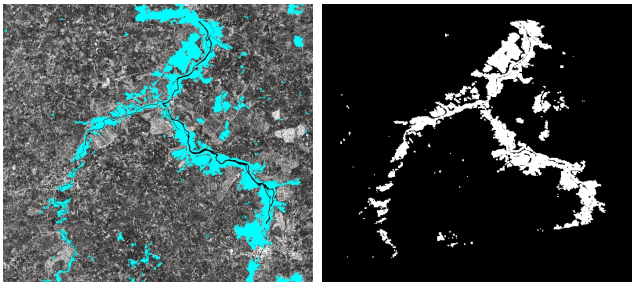

(a) (b)

Fig. 5. Ballinasloe test site, chain 2 results. (a) Retrieved flood map overlaid to the input GRD product. (b) Ground truth provided by ESA.

As for chain 2 (change-detection oriented) processing, some results, concerning the Ballinasloe test site (Ireland, EMS activation code: EMSR149) are reported in Figure 5. Even in this case, qualitatively, a good agreement with the available ground truth can be appreciated. However, the performance of the method have been evaluated also quantitatively, as reported in Table 2, and compared with those of other literature popular literature method like SVM, k-mean, NN, ML, and threshold applied to the ratio image. From the obtained results, concerning the aforementioned test sites, it arises that our method shows the better results in terms of the adopted quality parameters. In fact, average values registered for OA and Fa re the followings: Proposed method - OA: 92.0%, FA: 8.1%; SVM - OA: 67.7%, FA: 4.24%; k-mean - OA: 67.3%, FA: 15.9%; NN - OA: 75.0%, FA: 5.44%; Band ratio - OA: 80.7%, FA: 13.6%; ML - OA: 64.6%, FA: 4.09%.

Summarizing, the both the proposed processing chains give the best trade-off between detection rate and false alarms with respect to the tested literature methods, introducing also advantages concerning the lack of supervision and thresholding.

4. CONCLUSIONS

Rapid flood mapping is crucial for an effective event response. SAR sensors, thanks to their all-weather and all-time imaging capabilities, are a powerful instrument, able to provide timely information to first responders and decision makers. In this work, we presented a new methodology for unsupervised mapping of flooded areas introducing innovation both at product and at processing/methodological level. In fact, we exploit pre-processed Sentinel-1 ground range detected products provided by the European Space Agency, which are still poorly used in the SAR literature. They constitute the input for two successive processing levels with increasing computational burden, giving as output event maps with increasing resolution.

The first level accepts as input the post-event image, which is analyzed for standard Haralick textural features. Among them, the dissimilarity measure is exploited to feed a fuzzy flooding classification system. The system output is a map with 30 meters spatial resolution due to the applied moderate multilooking for speckle reduction.

The second processing level is based on change detection, exploiting a pre-event and a post-event GRD product. These images are combined into a change index feeding, together with the post-event amplitude information, the fuzzy classification system. The output is a flood map with 10 meters spatial resolution (i.e. the full resolution of the input products). The processing time depends on the selected despeckling algorithm. Both the level-one and level-two processing chain are fully unsupervised and threshold-free thanks to the adoption of fuzzy classification rules.

The performance of the proposed methodology were compared with those of several literature methods, both supervised and unsupervised. We showed that our method was able to outperform all of them providing the best trade-off between overall accuracy and false alarms.

The proposed method aims at providing end-users and decision makers with a new unsupervised tool for rapid flood mapping to support the first response to this kind of events.

5. ACKNOWLEDGMENTS

The authors thank the European Space Agency for making available the virtual machine exploited for basic preprocessing of Sentinel-1 images through the RSS Cloud Toolbox service.

Table 1. Comparison between RFP-L1 and other popular literature classification method: k-mean, support vector machine (SVM), neural net (NN), maximum likelihood (ML), and thresholding. DR: detection rate (percentage). FA: false alarms (percentage). Ground truth data available from the Copernicus Emergency Management Service. Bold characters indicate the best registered performance.

Dataset	Proposed		k-mean		SVM		NN		ML		Threshold	
	DR	FA	DR	FA	DR	FA	DR	FA	DR	FA	DR	FA
Ballinasloe	**94.5**	4.69	78.2	15.8	66.6	3.36	46.3	3.11	18.4	**2.31**	58.7	3.14
Selby	**92.1**	**1.00**	86.0	14.2	91.5	2.13	55.4	1.48	50.0	**1.00**	78.7	1.22
Poplar Bluff	**96.2**	7.33	91.7	15.7	92.2	5.00	62.7	3.00	67.5	1.84	63.7	**1.30**
Jemalong	**91.2**	13.3	65.4	21.0	64.6	5.00	33.6	4.44	35.6	4.33	33.1	**4.31**

Table 2. Comparison between RFP-L2 and other literature classification methods. SVM: support vector machine. NN: neural net. ML: maximum likelihood. BR: Band ratio. DR: detection rate (percentage). FA: false alarms (percentage). Ground truth data available from the Copernicus Emergency Management Service. Bold characters indicate the best registered performance.

Dataset	Proposed		k-mean		SVM		NN		ML		BR	
	DR	FA	DR	FA	DR	FA	DR	FA	DR	FA	DR	FA
Ballinasloe	**98.6**	6.60	59.1	21.9	64.6	3.94	80.9	4.70	51.4	**3.88**	96.6	6.45
Selby	91.8	**2.40**	90.2	21.2	90.5	3.39	**99.8**	6.71	94.0	2.72	95.7	29.5
Poplar Bluff	**84.1**	11.1	69.6	11.4	49.0	3.53	46.8	3.76	41.0	**3.19**	49.5	6.28
Jemalong	**93.6**	12.3	49.5	9.04	66.9	**6.11**	72.6	6.62	72.0	6.57	81.3	12.4

6. REFERENCES

[1] Committee on Earth Observation Satellites, "The Use of Earth Observing Satellites for Hazard Support: Assessments and Scenarios," U.S. Department of Commerce, National Oceanic and Atmospheric Administration, Tech. Rep., 2002.

[2] J. F. Rosser, D. G. Leibovici, and M. J. Jackson, "Rapid flood inundation mapping using social media, remote sensing and topographic data," *Natural Hazards*, vol. 87, no. 1, pp. 103–120, 2017.

[3] S. K. McFeeters, "The use of the Normalized Difference Water Index (NDWI) in the delineation of open water features," *Int. J. Remote Sens.*, vol. 17, no. 7, pp. 1425–1432, 1996.

[4] L. Pulvirenti, M. Chini, N. Pierdicca, and G. Boni, "Use of SAR data for detecting floodwater in urban and agricultural areas: The role of the interferometric coherence," *IEEE Transactions on Geoscience and Remote Sensing*, vol. 54, no. 3, pp. 1532–1544, 2016.

[5] F. Bovolo and L. Bruzzone, "A Split-Based Approach to Unsupervised Change Detection in Large-Size Multitemporal Images: Application to Tsunami Damage Assessment," *IEEE Trans. Geosci. Remote Sens.*, vol. 45, no. 6, pp. 1658–1670, 2007.

[6] D. Amitrano, F. Ciervo, G. Di Martino, M. N. Papa, A. Iodice, Y. Koussoube, F. Mitidieri, D. Riccio, and G. Ruello, "Modeling Watershed Response in Semiarid Regions with High Resolution Synthetic Aperture Radars," *IEEE J. Sel. Topics Appl. Earth Observ.*, vol. 7, no. 7, pp. 2732–2745, 2014.

[7] N. Gorelick, M. Hancher, M. Dixon, S. Ilyushchenko, D. Thau, and R. Moore, "Google Earth Engine: Planetary-scale geospatial analysis for everyone," *Remote Sensing of Environment*, In press.

[8] R. M. Haralick, K. Shanmugam, and I. H. Dinstein, "Textural Features for Image Classification," *IEEE Transactions on Systems, Man and Cybernetics*, vol. SMC-3, no. 6, pp. 610–621, 1973.

[9] D. Amitrano, G. Di Martino, A. Iodice, D. Riccio, and G. Ruello, "A New Framework for SAR Multitemporal Data RGB Representation: Rationale and Products," *IEEE Trans. Geosci. Remote Sens.*, vol. 53, no. 1, pp. 117–133, 2015.

[10] D. Amitrano, V. Belfiore, F. Cecinati, G. Di Martino, A. Iodice, P.-P. Mathieu, S. Medagli, D. Poreh, D. Riccio, and G. Ruello, "Urban Areas Enhancement in Multitemporal SAR RGB Images Using Adaptive Coherence Window and Texture Information," *IEEE J. Sel. Topics Appl. Earth Observ.*, vol. 9, no. 8, pp. 3740–3752, 2016.